

# Exceptional topology in Non-Hermitian Twisted Bilayer Graphene

Yingyi Huang<sup>1, 2, \*</sup>

<sup>1</sup>*School of Physics and Optoelectronic Engineering,*

*Guangdong University of Technology, Guangzhou 510006, China*

<sup>2</sup>*Guangdong Provincial Key Laboratory of Sensing Physics and System Integration Applications,*

*Guangdong University of Technology, Guangzhou, 510006, China*

(Dated: September 6, 2024)

Twisted bilayer graphene has extraordinary electronic properties at the magic angle along with an isolated flat band at magic angle. However, the non-Hermitian phenomena in twisted bilayer graphene remain unexplored. In this work, we study a non-Hermitian TBG formed by one-layer graphene twisted relative to another layer with gain and loss. Using a non-Hermitian generalization of Bistritzer-MacDonald(BM) model, we find Dirac cones centered at  $K'$  corner of the moiré Brillouin zone deformed in the presence of non-Hermiticity. This is different from single layer graphene with gain and loss, where rings of exceptional points appear in both  $K$  and  $K'$  corners of the Brillouin zone. The coincident of exceptional rings at  $\Gamma_M$  point characterizes an “exceptional magic angle”, at which the system hosts flat bands with zero energy and finite lifetime. More interestingly, we find that the topological charge in the moiré Brillouin zone is conserved during the expansion and fusion of the exceptional ring, which is absent in two-dimensional systems constraining by Nielsen-Ninomiya theorem. These findings can be demonstrated in realistic cold atom and metamaterial systems and will stimulate further study on non-Hermitian phenomena in twistronic.

## I. INTRODUCTION

Graphene owes extraordinary electronic and optical properties in two-dimensional (2D) systems [1, 2]. These properties relate to its lattice structure, which is directly interconnected with its wave-function topology. In single-layer graphene, the presence of unusual linear band dispersion termed Dirac band dispersion at  $K$  and  $K'$  points of the Brillouin zone is derived from its honeycomb lattice geometry. The Lorentz invariant Dirac cone at  $K$  and  $K'$  points are related by time-reversal symmetry and thus have opposite Berry phases, which has been confirmed in experiments [3, 4]. When two graphene layers are shifted with each other in rational competing periodicities upon shearing or twisting, they form a moiré pattern [5, 6]. One prominent example is a graphene bilayer with a relatively small angle rotation between the layers [7]. The recent studies on twisted bilayer graphene (TBG) focus on the extraordinary electronic properties at the magic angle along with an isolated flat band [8–12]. It is related to a variety of exotic phases including quantum anomalous Hall [13–17], fractional Chern insulators [18–20], ferromagnetic states [14, 21, 22], nematicity [23], unconventional superconductivity [24–29].

The topological properties of two-dimensional systems can be generalized to non-Hermitian systems by introducing on-site gain and loss [30–32]. The presence of non-Hermiticity can transform Hermitian degenerate points, such as a Dirac-like point or Weyl point, into a ring of exceptional points [33, 34]. At an exceptional point, not only the real and imaginary parts of the eigenvalues degenerate, but also the eigenvectors coalesce. Many phenomena are unique to non-Hermitian systems, including

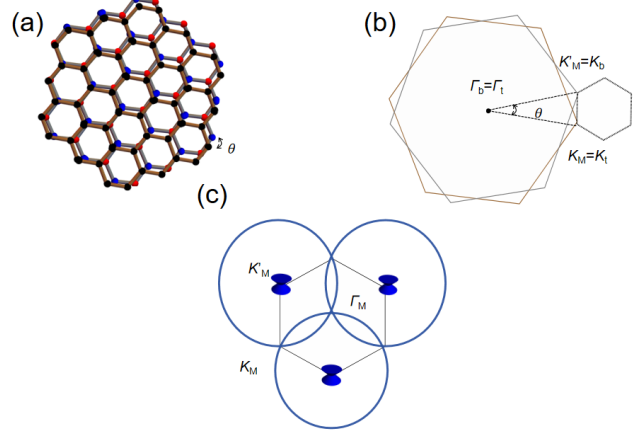


FIG. 1. (color online)Schematics of twisted bilayer graphene with onsite gain and loss. (a) Real-space geometrical picture: The gray (brown) honeycomb lattice marks the top (bottom) layer. The red (blue) dots represent the amplifying (lossy) sites in the bottom layer. (b) Momentum-space geometrical picture: The gray (brown) lattice marks the Brillouin zone of the top (bottom) layer graphene. Their expansion around the  $K$  valley forms a moiré Brillouin zone. (c) Moiré Brillouin zone physics: Under the effect of onsite gain and loss, Dirac points at  $K'_M$  points (related to  $K_b$  points of bottom layer graphene) morph into exceptional rings. At an “exceptional magic angle”, the exceptional rings touch at  $\Gamma_K$  point.

non-Hermitian skin effect [35] and non-Hermitian topological classifications [36, 37].

Despite topological robustness has been shown in one-dimensional moiré lattice under stain, the non-Hermitian effect of twisted moiré system with magic angle has been overlooked [38, 39].

In particular, twisted bilayer graphene has extraordinary topological properties. Since the two Dirac points in

\* yyhuang@gdut.edu.cn

moiré Brillouin zone (mBZ) in one valley emanate from different layers, their Berry phases can be identical due to the symmetry interlayer hopping term, which is generally not allowed in 2D periodic systems following the Nielsen-Ninomiya theorem [40, 41]. This is in contrast to single-layer graphene, in which the Berry phases of Dirac cones in different valleys has different topological charges. Actually, when the exceptional contours with opposite topological charges merge, the topological charge can be dissipated [34]. It is natural to ask how the exceptional geometry appears and develops in a non-Hermitian TBG system.

In this paper, we uncover a new type of twisted band engineering in TBG, with non-Hermitian perturbation on one of the layers. As shown in Fig. 1(a), balanced gain (in bright color) and loss (in light color) are put on the bottom layers (in red and blue, respectively). The superposing of two graphene layers with a twist angle between them creates moiré patterns. In the mBZ shown in Fig. 1(b), the low-energy band structure consists of Dirac cones from the rotated layers located at the  $K_M$  and  $K'_M$  corners. When the non-Hermitian perturbation is turned on the bottom layer, Dirac points morph into exceptional rings and the corresponding Dirac cones become exceptional cones, as shown in Fig. 1(c). We find that this non-Hermitian system hosts special angles for which multiple exceptional cones coincide at  $\Gamma_M$  points in an mBZ. We call this phenomenon “exceptional magic”. And importantly, our results demonstrated that the total Berry charge is conserved in the mBZ even after the merging of exceptional rings, this is a large difference from non-Hermitian single-layer graphene.

The paper is organized as follows. Section II introduces the non-Hermitian TBG model. Both the real and imaginary parts of the low-energy moiré band spectrum will be explored in Sec. III. In Sec. IV, we will use a non-Hermitian three triod model to discuss exceptional physics. In Sec. V, we calculate Beery curvature and the corresponding Chern number. Finally, we conclude our results in Sec. VI.

## II. THE NON-HERMITIAN BILAYER MODEL

We consider balanced gain and loss on both layers of the bilayer system. We can write down a non-Hermitian generalization of the single-valley model for twisted bilayer graphene. The low-energy Hamiltonian for the  $K$  mBZ is:

$$H = \begin{pmatrix} h_b(\mathbf{k}) & \mathbf{T}(\mathbf{r}) \\ \mathbf{T}(\mathbf{r})^\dagger & h_t(\mathbf{k}) \end{pmatrix} \quad (1)$$

where the top layer Hamiltonian is

$$h_t = -iv_F \boldsymbol{\sigma}_{\theta/2} \nabla \quad (2)$$

and the bottom layer Hamiltonian is non-Hermitian

$$h_b = -iv_F \boldsymbol{\sigma}_{-\theta/2} \nabla + i\lambda_V \sigma_z. \quad (3)$$

Here,  $i\lambda_V \sigma_z$  is a balanced gain and loss imposing on the bottom layer, which induces non-Hermiticity. And  $\boldsymbol{\sigma}_{\theta/2}$  corresponds to the rotated Pauli matrices  $e^{-i\theta\sigma_z/4}(\sigma_x, \sigma_y)e^{i\theta\sigma_z/4}$ .  $\mathbf{T}(\mathbf{r}) = \sum_{j=1}^3 T_j e^{-ik_\theta \mathbf{q}_j \cdot \mathbf{r}}$  is the sublattice-dependent moiré potential that couples the two layers. The interlayer coupling is in the form

$$T_{j+1} = w_0 \sigma + w_1 (\sigma_x \cos j\phi + \sigma_y \sin j\phi) \quad (4)$$

with  $\phi = 2\pi/3$  and  $w_0 (w_1)$  the interlayer coupling strength in the AA (AB) region. The unit vectors  $\mathbf{q}_1 = (0, -1)$ ,  $\mathbf{q}_{2,3} = (\pm\sqrt{3}/2, 1/2)$ .  $k_\theta = 2k_D \sin(\theta/2)$  is the moiré modulation vector and  $k_D = 4\pi/(3a_0)$  is the magnitude of the Dirac wave vector, where  $a_0$  is the lattice constant of monolayer graphene. The hopping strength  $w$  encodes the inter-layer coupling in the AB region.

The generators of the magnetic space group  $P6'2'2$  for the Hermitian twisted bilayer graphene include a  $C_{3z} = e^{i\frac{2\pi}{3}\sigma_z}$  rotation symmetry, a  $C_{2x} = \tau_x \sigma_x$  rotation symmetry, and a  $C_{2z}T = \sigma_z \mathcal{K}$  symmetry [42]. The single-valley Hamiltonian only has the  $C_{3z}$  symmetry, since  $C_{2z}$  and  $T$  symmetries play the role of mapping one valley to the other. We can check that the non-Hermitian model preserves the  $C_{3z}$  rotation symmetry.

If there is no AA stacking ( $u = 0$ ), the Hamiltonian preserves chiral symmetry  $\mathcal{CH}(\mathbf{r})\mathcal{C}^\dagger = -\mathcal{H}(\mathbf{r})$  under chiral symmetry operator  $\mathcal{C} = \sigma_z$  in the absence of non-Hermiticity [42–44, 46].

In the presence of the balanced gain and loss  $i\sigma_z$  term, the chiral symmetry is broken but non-Hermitian chiral symmetry is preserved. In the following numerical calculation, we take  $\hbar v_F/a = 2380\text{meV}$ ,  $w_1 = 110\text{meV}$  and  $2v_0 k_D = 19.81\text{eV}$ . They correspond to the first magic angle  $\alpha \approx 0.586$ .

## III. THE APPEARANCE AND DEVELOPMENT OF EXCEPTIONAL RINGS

Let us investigate the band structure for twist angle  $\theta = 1$ . In the absence of non-Hermiticity, this is not a magic angle with a flat band. If the interlayer coupling effect is absent ( $w_0 = w_1 = 0$ ), the dispersion in the moiré Brillouin zone is equivalent to the folded dispersion in the Brillouin zone of graphene. The Dirac point of the  $K$  point in layer 1 is mapped to  $K_M$ , while that of the  $K'$  point of layer 2 is mapped to  $K'_M$ .

In the presence of non-Hermitian perturbation  $\lambda_V$ , the energy dispersion becomes complex. In Fig. 2(a), we can see that non-Hermitian perturbation deforms the Dirac cones at  $K'_M$  corners. More specifically, the degeneracy point at the  $K'_M$  points in the real part of the spectrum morphs into a ring of degeneracy points. This is a stark difference from single-layer graphene with onsite gain and loss. The latter has deformed Dirac cones in both  $K$  and  $K'$  corners in the Brillouin zone. This difference is due to the fact that  $K_M$  and  $K'_M$  in non-Hermitian TBG are

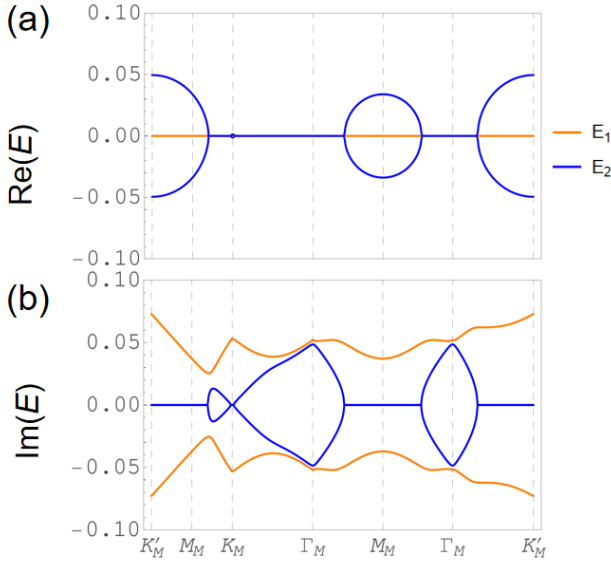


FIG. 2. (Color online) (a) The real part and (b) the imaginary part of the band spectra in the mBZ for  $\theta = 1$ ,  $u_0 = 0$ ,  $u_1 = 0.005$ ,  $\lambda_V = 0.05$ .

folded from different graphene layers. The non-Hermitian  $\lambda_V$  can only deform the Dirac cone on the bottom layer.

In particular, the degeneracy of the two lowest energy states leads to the appearance of singularity points in momentum space. At the same time, a ring of degeneracy point appears at the same momentum position in the imaginary part of the spectrum, as shown in Fig. 2(b). We found that not only the eigenvalues coalesce but also their corresponding eigenvectors coalesce at this point. This confirms that these singularity points are exceptional points in momentum space. Thus, the Dirac cone is turned into a ring of exceptional points, this is similar to that in non-Hermitian semimetals [33].

At a critical non-Hermitian strength, the exceptional point approach  $\Gamma_M$  point, where the whole lowest band becomes flat, as shown in Fig. 3. Different metric including the vanishing of Dirac velocity, maximum gap to neighboring bands, and minimum bandwidth gives the same results. The value of this critical non-Hermiticity strength  $\lambda_{Vc}$  depends on the twist angle  $\theta$ .

#### IV. EXCEPTIONAL CONE

To understand the nonhermitian physics, we use the simplified tripod mode model [8], which truncates Eq. ?? at the first honeycomb shell. The Hamiltonian is written as

$$H_{Tri} = \begin{pmatrix} h_b(\mathbf{k}) & T_1 & T_2 & T_3 \\ T_1 & h_{t1}(\mathbf{k} - \mathbf{q}_1) & 0 & 0 \\ T_2 & 0 & h_{t2}(\mathbf{k} - \mathbf{q}_2) & 0 \\ T_3 & 0 & 0 & h_{t3}(\mathbf{k} - \mathbf{q}_3) \end{pmatrix} \quad (5)$$

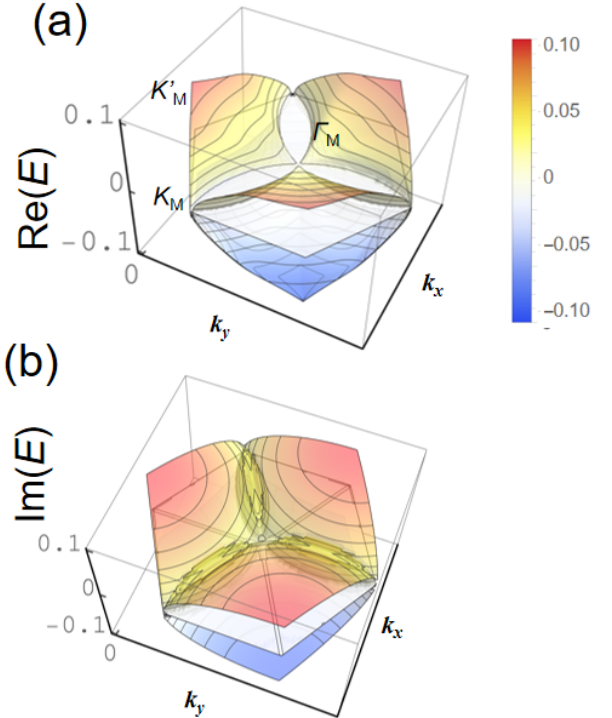


FIG. 3. (color online) (a) The real part and (b) the imaginary part of the four lowest bands in the mBZ for  $u_0 = 0$ ,  $u_1 = 0.005$ ,  $\lambda_V = 0.072$ . The real parts of the two lowest bands are flat.

where  $h_{tj}$  for  $j = 1, 2, 3$  are on the top layer and  $h_b$  on the bottom layer. Since  $h_b$  is non-Hermitian, the Hamiltonian  $H_{Tri}$  has biorthogonal eigenvectors. In this system, the left and right eigenvectors are four two-component spinors

$$\Psi_\alpha^T(\mathbf{k}) = (\psi_0(\mathbf{k}), \psi_1(\mathbf{k}), \psi_2(\mathbf{k}), \psi_3(\mathbf{k}))_\alpha^T, \quad \alpha = L, R. \quad (6)$$

Using perturbation theory one can derived the effective Hamiltonian in the space of  $\psi_0$ . The Hamiltonian can be divided into a momentum-independent part  $\mathcal{H}^{(0)}$  and a momentum-dependent part  $\mathcal{H}_k^{(1)}$ . The  $\psi_{jR}$  can be expressed by

$$\psi_{jR} = -h_j^{-1} T_j \psi_{0R}. \quad (7)$$

Since  $h_j$  is independent of non-Hermiticity, we can expect  $T_j h_j^{-1} T_j = 0$ , which is similar to the Hermitian model. Thus, the  $\psi_0$  spinor in the zero-energy eigenstates satisfies

$$\psi_0 \psi_{0R} = 0. \quad (8)$$

This form seems to be the same as that of the Hermitian TBG. However,  $h_0$  is in a non-Hermitian form, the  $\psi_{0R}$  is different from  $\psi_{0L}$ . We can check that the biorthogonal wave functions are normalized as

$$\langle \Psi_{0L} | \Psi_{0R} \rangle = 1 + 3(\alpha_0^2 + \alpha_1^2). \quad (9)$$

The effective Hamiltonian matrix to leading order in  $k$  is

$$\Psi^{(i)}|\mathcal{H}_{\mathbf{k}}^{(1)}|\Psi^{(j)}\rangle = \psi_0^{(i)\dagger}(-v_F^*\sigma \cdot \mathbf{k} + i\lambda^*\sigma_z)\psi_0^{(j)} \quad (10)$$

with the renormalized velocity being

$$\frac{v_F^*}{v_F} = \frac{1 - 3\alpha_1^2}{1 + 3(\alpha_0^2 + \alpha_1^2)} \quad (11)$$

and the renormalized non-Hermitian strength being

$$\frac{\lambda^*}{\lambda} = \frac{1 - 3(\alpha_0^2 - \alpha_1^2)}{1 + 3(\alpha_0^2 + \alpha_1^2)}. \quad (12)$$

We can see that aside from a renormalized velocity and non-Hermitian strength, the form of Hamiltonian is identical to the continuum model Hamiltonian of non-Hermitian single-layer graphene. The form of the renormalized velocity is the same as that of the Hermitian TBG. It decreases with increasing interlayer coupling in AB region  $\alpha_1$ . To see the effect of interlayer coupling on non-Hermitian strength, we should discuss two cases. When  $\alpha_0 = 0$ ,  $\lambda^*$  increases with increasing interlayer coupling in AB region  $\alpha_1$ . Thus, the ratio  $\lambda^*/v_F^*$  becomes larger as  $\alpha_1$  increases. When  $\alpha_0 \neq 0$ ,  $\lambda^*$  increases

with increasing interlayer coupling in AA region  $\alpha_0$ . The non-Hermitian effect is more complicated.

## V. BERRY CURVATURE AND CHERN NUMBER

So far, we have shown the existence of exceptional geometries in the non-Hermitian TBG. In this section, we will explore their topological properties numerically.

The topological charge or Chern number of an exceptional contour can be obtained by integrating the Berry connection  $A(\mathbf{k})$  along a closed surface containing the exceptional contour

$$\mathcal{C} = \frac{1}{2\pi} \oint_{\partial S} \mathbf{A}(\mathbf{k}) \cdot d\mathbf{k} = \frac{1}{2\pi} \int_S \Omega(\mathbf{k}) \cdot d\mathbf{S}, \quad (13)$$

where the Berry connection is defined by the eigenvectors as

$$\mathbf{A}^{\beta, \beta'} = i\langle\psi^\beta(\mathbf{k})|\nabla_{\mathbf{k}}|\psi^{\beta'}(\mathbf{k})\rangle. \quad (14)$$

Here,  $|\psi^{\beta'}(\mathbf{k})\rangle$  and  $\langle\psi^\beta(\mathbf{k})|$  can be the left or right eigenvectors. Since previous study has proven that the total topological charge is the same for four possible choices of eigenvectors [47], we will choose  $\beta = L$  and  $\beta' = R$  in the following calculation.

In numerical calculation, the Berry connection is presented by the local Berry curvature  $\Omega(\mathbf{k}) = \nabla_{\mathbf{k}} \times \mathbf{A}(\mathbf{k})$ , which can be calculated as

$$\Omega(\mathbf{k})^{\beta, \beta'} = \lim_{q \rightarrow 0} \frac{1}{4q^2} \langle\psi_{\mathbf{k}-q\hat{x}-q\hat{y}}^{\beta'}|\psi_{\mathbf{k}-q\hat{x}+q\hat{y}}^{\beta}\rangle \langle\psi_{\mathbf{k}-q\hat{x}+q\hat{y}}^{\beta'}|\psi_{\mathbf{k}+q\hat{x}+q\hat{y}}^{\beta}\rangle \langle\psi_{\mathbf{k}+q\hat{x}+q\hat{y}}^{\beta'}|\psi_{\mathbf{k}+q\hat{x}-q\hat{y}}^{\beta}\rangle \langle\psi_{\mathbf{k}+q\hat{x}-q\hat{y}}^{\beta'}|\psi_{\mathbf{k}-q\hat{x}-q\hat{y}}^{\beta'}\rangle \quad (15)$$

with  $q$  being half of the lattice constant.

Figure 4 shows the Berry curvature in mBZ. We can see that Berry curvatures have sharp peaks around  $\Gamma_M - K_M$  high symmetric lines, which are close to the boundary of exceptional rings. This can be well understood since Berry curvature is the phase of an overlap tracing a small loop in mBZ. On the boundary of exceptional rings, the wave functions vary rapidly and will give a large Berry curvature.

Upon summing the Berry curvature on the mBZ, we can obtain the total Berry charge or Chern number

$$\mathcal{C} = \sum_{mBZ} \Omega^{LR}(\mathbf{k}). \quad (16)$$

The non-Hermitian perturbation transforms a Dirac point into an exceptional ring. In the mBZ, there are three-thirds of exceptional rings from Dirac points in different moiré corners. We find that the total Berry charge in mBZ is 1 throughout the merging of exceptional rings with increasing  $\lambda_V$  (e.g.,  $0 \leq \lambda_V \leq 0.85$  for  $\theta = 1$ ). At

much larger  $\lambda_V$ , the Berry charge can be a quantized value larger than 1 due to approaching band crossings with the remote bands. This supports our expectation that the topological charge in the system is preserved in the exceptional contour. And most importantly, this characterizes the topological features of non-Hermitian TBG. This is opposite to the merging of exceptional contours with opposite topological charge, in which the topological charge is dissipated and gives a single, uncharged exceptional contour.

## VI. DISCUSSION AND CONCLUSION

In this paper, we have studied a non-Hermitian generalization of twisted bilayer graphene system with balanced gain and loss on one of the layers. We found that exceptional rings centered at  $K'$  corner in the moiré Brillouin zone in the  $K(K')$  valley. This is due to the folding of the Brillouin zone, and it is absent in the single-layer

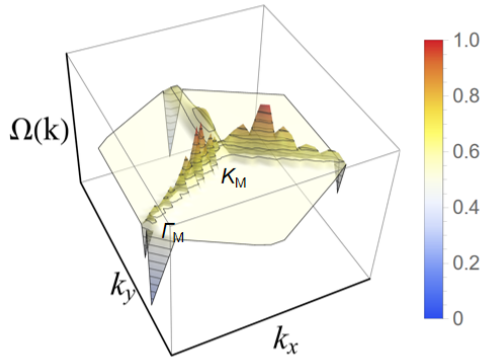


FIG. 4. (color online) Berry curvature for the  $\sigma_z = 1$  band in the moiré Brillouin zone for  $u_0 = 0$ ,  $u_1 = 0.005$ ,  $\theta = 1$  and  $\lambda_V = 0.08 > \lambda_{Vc}$ . A small in-plane electric field is imposed to open the gap.

graphene. The exceptional rings coincide and form bands whose real parts are flat at a specific non-Hermitian strength, which is denoted as “exceptional Dirac magic”. This flat band is characterized with a robust Chern number  $\mathcal{C} = 1$  in moiré Brillouin zone. This is different from single-layer graphene in which Dirac/Weyl exceptional rings carrying opposite topological charges are coupled and annihilated.

We have introduced a new design concept for twisted moiré systems, in which a certain “exceptional Dirac magic” angle is achieved. Non-Hermitian TBG can be realized in cold atom and metamaterial system. On one hand, due to the great advantage of manipulating atom-atom interaction and light-matter coupling, ultracold atom experiments provide an unprecedented opportunity.

Remarkably, atomic Bose-Einstein condensate has been recently realized in twisted bilayer optical lattices [57]. Also, there are proposals on the photonic analog [48–52] and phononic analog [53, 54] of twisted bilayer graphene. In particular, there is demonstration of optical bilayer photonic crystal devices in the microwave range [55] and in the optical frequency range [56]. On the other hand, on-site dissipations are well-controlled non-Hermitian terms that can be realized experimentally in many systems [30–32]. In particular, the Weyl exceptional ring has been realized in photonic experiment [58, 59].

The highlight of this work is the discovery of non-dissipation exceptional topology. The interplay of topology, non-Hermitian, and moiré physics can open the door to new phenomena. Especially, the reduced kinetic energy of the flat bands in twisted bilayer graphene makes it a correlated system. Non-Hermitian strongly interacting Dirac system has recently been calculated [60]. The non-Hermitian physics in quantum many-body systems, such as strongly correlated phases in moiré system, will be a future focus.

Note added-. Upon completion of our manuscript, we became aware of a recent paper on non-Hermitian twisted bilayer graphene, in which non-Hermiticity is on the hopping amplitude and topological aspects are undiscussed.

## ACKNOWLEDGMENTS

This work is supported by the National Natural Science Foundation of China (Grant No. 12104099 and No. 12274095) and Guangzhou Science and Technology Program (Grant No. 2024A04J0272)

---

[1] A. C. Neto, F. Guinea, N. M. Peres, K. S. Novoselov, and A. K. Geim, The electronic properties of graphene, *Reviews of modern physics* **81**, 109 (2009).

[2] P. A. D. Gonçalves and N. M. Peres, *An introduction to graphene plasmonics* (World Scientific, 2016).

[3] K. S. Novoselov, A. K. Geim, S. V. Morozov, D. Jiang, M. I. Katsnelson, I. V. Grigorieva, S. V. Dubonos, and A. A. Firsov, Two-dimensional gas of massless dirac fermions in graphene, *nature* **438**, 197 (2005).

[4] Y. Zhang, Y.-W. Tan, H. L. Stormer, and P. Kim, Experimental observation of the quantum hall effect and berry’s phase in graphene, *nature* **438**, 201 (2005).

[5] J.-C. Charlier, J.-P. Michenaud, and P. Lambin, Tight-binding density of electronic states of pregraphitic carbon, *Phys. Rev. B* **46**, 4540 (1992).

[6] E. McCann, Asymmetry gap in the electronic band structure of bilayer graphene, *Phys. Rev. B* **74**, 161403 (2006).

[7] J. L. Dos Santos, N. Peres, and A. C. Neto, Graphene bilayer with a twist: electronic structure, *Physical review letters* **99**, 256802 (2007).

[8] R. Bistritzer and A. H. MacDonald, Moiré bands in twisted double-layer graphene, *Proceedings of the National Academy of Sciences* **108**, 12233 (2011).

[9] R. Bistritzer and A. MacDonald, Moiré butterflies in twisted bilayer graphene, *Physical Review B* **84**, 035440 (2011).

[10] J. L. Dos Santos, N. Peres, and A. C. Neto, Continuum model of the twisted graphene bilayer, *Physical Review B* **86**, 155449 (2012).

[11] S. Shallcross, S. Sharma, E. Kandelaki, and O. A. Pankratov, Electronic structure of turbostratic graphene, *Phys. Rev. B* **81**, 165105 (2010).

[12] A. Luican, G. Li, A. Reina, J. Kong, R. Nair, K. S. Novoselov, A. K. Geim, and E. Andrei, Single-layer behavior and its breakdown in twisted graphene layers, *Physical review letters* **106**, 126802 (2011).

[13] M. Serlin, C. Tschirhart, H. Polshyn, Y. Zhang, J. Zhu, K. Watanabe, T. Taniguchi, L. Balents, and A. Young, Intrinsic quantized anomalous hall effect in a moiré heterostructure, *Science* **367**, 900 (2020).

[14] A. L. Sharpe, E. J. Fox, A. W. Barnard, J. Finney, K. Watanabe, T. Taniguchi, M. Kastner, and D. Goldhaber-Gordon, Emergent ferromagnetism near three-quarters filling in twisted bilayer graphene,

Science **365**, 605 (2019).

[15] K. P. Nuckolls, M. Oh, D. Wong, B. Lian, K. Watanabe, T. Taniguchi, B. A. Bernevig, and A. Yazdani, Strongly correlated chern insulators in magic-angle twisted bilayer graphene, *Nature* **1** (2020).

[16] S. Wu, Z. Zhang, K. Watanabe, T. Taniguchi, and E. Y. Andrei, Chern insulators, van hove singularities and topological flat bands in magic-angle twisted bilayer graphene, *Nature materials* **20**, 488 (2021).

[17] Y. Choi, H. Kim, Y. Peng, A. Thomson, C. Lewandowski, R. Polski, Y. Zhang, H. S. Arora, K. Watanabe, T. Taniguchi, *et al.*, Correlation-driven topological phases in magic-angle twisted bilayer graphene, *Nature* **589**, 536 (2021).

[18] Y. Xie, A. T. Pierce, J. M. Park, D. E. Parker, E. Khalaf, P. Ledwith, Y. Cao, S. H. Lee, S. Chen, P. R. Forrester, *et al.*, Fractional chern insulators in magic-angle twisted bilayer graphene, *Nature* **600**, 439 (2021).

[19] H. Park, J. Cai, E. Anderson, Y. Zhang, J. Zhu, X. Liu, C. Wang, W. Holtzmann, C. Hu, Z. Liu, *et al.*, Observation of fractionally quantized anomalous Hall effect, *Nature* **622**, 74 (2023).

[20] Z. Lu, T. Han, Y. Yao, A. P. Reddy, J. Yang, J. Seo, K. Watanabe, T. Taniguchi, L. Fu, and L. Ju, Fractional quantum anomalous hall effect in a graphene moire superlattice, *arXiv preprint arXiv:2309.17436* (2023).

[21] Y. Saito, J. Ge, L. Rademaker, K. Watanabe, T. Taniguchi, D. A. Abanin, and A. F. Young, Hofstadter subband ferromagnetism and symmetry-broken chern insulators in twisted bilayer graphene, *Nature Physics* **17**, 478 (2021).

[22] J.-X. Lin, Y.-H. Zhang, E. Morissette, Z. Wang, S. Liu, D. Rhodes, K. Watanabe, T. Taniguchi, J. Hone, and J. Li, Spin-orbit–driven ferromagnetism at half moiré filling in magic-angle twisted bilayer graphene, *Science* **375**, 437 (2022).

[23] Y. Cao, D. Rodan-Legrain, J. M. Park, N. F. Yuan, K. Watanabe, T. Taniguchi, R. M. Fernandes, L. Fu, and P. Jarillo-Herrero, Nematicity and competing orders in superconducting magic-angle graphene, *science* **372**, 264 (2021).

[24] Y. Cao, V. Fatemi, A. Demir, S. Fang, S. L. Tomarken, J. Y. Luo, J. D. Sanchez-Yamagishi, K. Watanabe, T. Taniguchi, E. Kaxiras, *et al.*, Correlated insulator behaviour at half-filling in magic-angle graphene superlattices, *Nature* **556**, 80 (2018).

[25] Y. Cao, V. Fatemi, S. Fang, K. Watanabe, T. Taniguchi, E. Kaxiras, and P. Jarillo-Herrero, Unconventional superconductivity in magic-angle graphene superlattices, *Nature* **556**, 43 (2018).

[26] M. Yankowitz, S. Chen, H. Polshyn, Y. Zhang, K. Watanabe, T. Taniguchi, D. Graf, A. F. Young, and C. R. Dean, Tuning superconductivity in twisted bilayer graphene, *Science* **363**, 1059 (2019).

[27] E. Khalaf, S. Chatterjee, N. Bultinck, M. P. Zaletel, and A. Vishwanath, Charged skyrmions and topological origin of superconductivity in magic-angle graphene, *Science advances* **7**, eabf5299 (2021).

[28] S. Chatterjee, M. Ippoliti, and M. P. Zaletel, Skyrmion superconductivity: DMRG evidence for a topological route to superconductivity, *Phys. Rev. B* **106**, 035421 (2022).

[29] P. Törmä, S. Peotta, and B. A. Bernevig, Superconductivity, superfluidity and quantum geometry in twisted multilayer systems, *Nature Reviews Physics* **4**, 528 (2022).

[30] K. Ding, C. Fang, and G. Ma, Non-hermitian topology and exceptional-point geometries, *Nature Reviews Physics* **4**, 745 (2022).

[31] Y. Ashida, Z. Gong, and M. Ueda, Non-hermitian physics, *Advances in Physics* **69**, 249 (2020).

[32] E. J. Bergholtz, J. C. Budich, and F. K. Kunst, Exceptional topology of non-hermitian systems, *Reviews of Modern Physics* **93**, 015005 (2021).

[33] Y. Xu, S.-T. Wang, and L.-M. Duan, Weyl exceptional rings in a three-dimensional dissipative cold atomic gas, *Physical review letters* **118**, 045701 (2017).

[34] A. Cerjan, M. Xiao, L. Yuan, and S. Fan, Effects of non-hermitian perturbations on weyl hamiltonians with arbitrary topological charges, *Physical Review B* **97**, 075128 (2018).

[35] S. Yao and Z. Wang, Edge states and topological invariants of non-hermitian systems, *Physical review letters* **121**, 086803 (2018).

[36] K. Kawabata, K. Shiozaki, M. Ueda, and M. Sato, Symmetry and topology in non-hermitian physics, *Physical Review X* **9**, 041015 (2019).

[37] Z. Gong, Y. Ashida, K. Kawabata, K. Takasan, S. Higashikawa, and M. Ueda, Topological phases of non-hermitian systems, *Physical Review X* **8**, 031079 (2018).

[38] K. Shao, H. Geng, E. Liu, J. L. Lado, W. Chen, and D. Xing, Non-hermitian moiré valley filter, *Physical Review Letters* **132**, 156301 (2024).

[39] Y.-R. Zhang, Z.-Z. Zhang, J.-Q. Yuan, M. Kang, and J. Chen, High-order exceptional points in non-hermitian moire lattices, *Frontiers of Physics* **14**, 1 (2019).

[40] J. Ahn, S. Park, and B.-J. Yang, Failure of nielsen-ninomiya theorem and fragile topology in two-dimensional systems with space-time inversion symmetry: Application to twisted bilayer graphene at magic angle, *Phys. Rev. X* **9**, 021013 (2019).

[41] H. B. Nielsen and M. Ninomiya, *No-go theorem for regularizing chiral fermions*, Tech. Rep. (Science Research Council, 1981).

[42] Z.-D. Song, B. Lian, N. Regnault, and B. A. Bernevig, Twisted bilayer graphene. ii. stable symmetry anomaly, *Physical Review B* **103**, 205412 (2021).

[43] S. Carr, S. Fang, Z. Zhu, and E. Kaxiras, Exact continuum model for low-energy electronic states of twisted bilayer graphene, *Physical Review Research* **1**, 013001 (2019).

[44] G. Tarnopolsky, A. J. Kruchkov, and A. Vishwanath, Origin of magic angles in twisted bilayer graphene, *Physical review letters* **122**, 106405 (2019).

[45] N. N. T. Nam and M. Koshino, Lattice relaxation and energy band modulation in twisted bilayer graphene, *Phys. Rev. B* **96**, 075311 (2017).

[46] G. Tarnopolsky, A. J. Kruchkov, and A. Vishwanath, Origin of magic angles in twisted bilayer graphene, *Phys. Rev. Lett.* **122**, 106405 (2019).

[47] H. Shen, B. Zhen, and L. Fu, Topological band theory for non-hermitian hamiltonians, *Physical review letters* **120**, 146402 (2018).

[48] M. Oudich, G. Su, Y. Deng, W. Benalcazar, R. Huang, N. J. R. K. Gerard, M. Lu, P. Zhan, and Y. Jing, Photonic analog of bilayer graphene, *Phys. Rev. B* **103**, 214311 (2021).

[49] B. Lou, N. Zhao, M. Minkov, C. Guo, M. Orenstein, and

S. Fan, Theory for twisted bilayer photonic crystal slabs, *Phys. Rev. Lett.* **126**, 136101 (2021).

[50] S. Sunku, G. Ni, B.-Y. Jiang, H. Yoo, A. Sternbach, A. McLeod, T. Stauber, L. Xiong, T. Taniguchi, K. Watanabe, *et al.*, Photonic crystals for nano-light in moiré graphene superlattices, *Science* **362**, 1153 (2018).

[51] Y. Deng, M. Oudich, N. J. Gerard, J. Ji, M. Lu, and Y. Jing, Magic-angle bilayer phononic graphene, *Physical Review B* **102**, 180304 (2020).

[52] C. Valagiannopoulos, Electromagnetic analog to magic angles in twisted bilayers of two-dimensional media, *Physical Review Applied* **18**, 044011 (2022).

[53] M. Oudich, Y. Deng, and Y. Jing, Twisted pillared phononic crystal plates, *Applied Physics Letters* **120** (2022).

[54] S. M. Gardezi, H. Pirie, S. Carr, W. Dorrell, and J. E. Hoffman, Simulating tristronics in acoustic metamaterials, *2D Materials* **8**, 031002 (2021).

[55] B. Lou, B. Wang, J. A. Rodríguez, M. Cappelli, and S. Fan, Tunable guided resonance in twisted bilayer photonic crystal, *Science Advances* **8**, eadd4339 (2022).

[56] H. Tang, B. Lou, F. Du, M. Zhang, X. Ni, W. Xu, R. Jin, S. Fan, and E. Mazur, Experimental probe of twist angle-dependent band structure of on-chip optical bilayer photonic crystal, *Science Advances* **9**, eadh8498 (2023).

[57] Z. Meng, L. Wang, W. Han, F. Liu, K. Wen, C. Gao, P. Wang, C. Chin, and J. Zhang, Atomic bose-einstein condensate in twisted-bilayer optical lattices, *Nature* **615**, 231 (2023).

[58] A. Cerjan, S. Huang, M. Wang, K. P. Chen, Y. Chong, and M. C. Rechtsman, Experimental realization of a weyl exceptional ring, *Nature Photonics* **13**, 623 (2019).

[59] W. Song, S. Wu, C. Chen, Y. Chen, C. Huang, L. Yuan, S. Zhu, and T. Li, Observation of weyl interface states in non-hermitian synthetic photonic systems, *Physical Review Letters* **130**, 043803 (2023).

[60] X.-J. Yu, Z. Pan, L. Xu, and Z.-X. Li, Non-hermitian strongly interacting dirac fermions, *Physical Review Letters* **132**, 116503 (2024).